Dalton Transactions

ROYAL SOCIETY OF CHEMISTRY

PAPER

View Article Online
View Journal | View Issue

Cite this: *Dalton Trans.*, 2026, **55**, 4108

Cyclam-based Cu(II) and Fe(III) complexes for antifouling coating development

Inês M. Nunes,[a,b] Bruno J. C. Vieira,[c,d,e] João C. Waerenborgh,[c,d,e] Maria J. Romeu,[f,g] Rita Teixeira-Santos,[f,g] Ana P. Carapeto,[b,h] Noelia Losada-García,[b] Filipe J. Mergulhão,[f,g] Elisabete R. Silva *[b,i] and Luis G. Alves *[b,j]

Received 18th July 2025,
Accepted 9th February 2026

DOI: 10.1039/d5dt01700a

rsc.li/dalton

Biofouling, the accumulation of microorganisms and macroorganisms on submerged surfaces, is responsible for equipment degradation and increased maintenance costs. Several efforts have been made for the development of efficient antifouling surfaces, but most coating formulations are still based on toxic and harmful compounds. This study evaluated the effectiveness of polyurethane (PU) coatings modified with cyclam-based Cu(II) and Fe(III) complexes in preventing *Cobetia marina* biofilm formation under controlled hydrodynamic conditions mimicking marine environments. The modified PU-based coatings incorporating these complexes showed promising results in reducing biofilm thickness (17–38%), biofilm total volume (33–39%) and culturable biofilm cells (36–39%) compared to the unmodified PU control. These findings demonstrate that cyclam-based Cu(II) and Fe(III) complexes are effective antifouling agents for marine applications due to their low ecotoxicity and compatibility with polymeric formulations.

Introduction

Marine biofouling is an undesirable process in which submerged or water-contacting surfaces are progressively covered with organisms and their metabolic by-products. This process begins with the formation of a biofilm (microfouling or slime), which is spontaneously colonized by microorganisms such as bacteria, algae, and protozoa. This microbial layer creates favourable conditions for the attachment and growth of larger fouling organisms, including invertebrates like barnacles and mussels, as well as macroalgae. The result is a complex biological accumulation that severely compromises the performance and longevity of marine infrastructures.[1]

In the marine transport sector, particularly in commercial shipping, biofouling is a major operational burden. The accumulation of biological material on hull surfaces can increase roughness and hydrodynamic drag, leading to higher fuel consumption. These efficiency losses, combined with costs related to hull cleaning, dry-docking, and unscheduled maintenance, are estimated to cause large economic losses in global maritime transportation annually.[2] The environmental consequences are equally concerning, as biofouling remains a primary pathway for the spread of invasive marine species, posing serious threats to local ecosystems and marine biodiversity.[3]

Antifouling protection has relied mostly on coatings containing organotin complexes that inhibit organisms' growth through metal ion release. Although these systems are effective, uncontrolled metal leaching has raised major environmental concerns. Solutions for biofouling control have been explored in the development of efficient and environmentally friendly coatings to replace the current toxic biocide-based strategies.[4] Polymeric antifouling coatings that incorporate one or more bioactive compounds are being successfully used to inhibit or prevent the adhesion and growth of aquatic

[a]*Centro de Química Estrutural, Instituto Superior Técnico, Universidade de Lisboa, Av. Rovisco Pais 1, 1049-001 Lisboa, Portugal*
[b]*BioISI – Biosystems & Integrative Sciences Institute, Faculdade de Ciências da Universidade de Lisboa, Campo Grande, 1749-016 Lisboa, Portugal. E-mail: ersilva@ciencias.ulisboa.pt, luis.g.alves@tecnico.ulisboa.pt*
[c]*Departamento de Engenharia e Ciências Nucleares (DECN), Instituto Superior Técnico, Universidade de Lisboa, Estrada Nacional 10, Bobadela, 2695-066 Loures, Portugal*
[d]*Centro de Física e Engenharia de Materiais Avançados (CeFEMA), Instituto Superior Técnico, Universidade de Lisboa, Av. Rovisco Pais 1, 1049-001 Lisbon, Portugal*
[e]*Laboratory of Physics for Materials and Emergent Technologies (LaPMET), Av. Rovisco Pais 1, 1049-001 Lisbon, Portugal*
[f]*LEPABE – Laboratory for Process Engineering, Environment, Biotechnology and Energy, Faculty of Engineering, University of Porto, Rua Dr. Roberto Frias, 4200-465 Porto, Portugal*
[g]*ALiCE – Associate Laboratory in Chemical Engineering, Faculty of Engineering, University of Porto, Rua Dr. Roberto Frias, 4200-465 Porto, Portugal*
[h]*Departamento de Física, Faculdade de Ciências, Faculty of Sciences, University of Lisboa, Campo Grande, 1749-016 Lisboa, Portugal*
[i]*Departamento de Química e Bioquímica, Faculdade de Ciências, Universidade de Lisboa, Campo Grande, 1749-016 Lisboa, Portugal*
[j]*Centro de Química Estrutural, Institute of Molecular Sciences, Associação do Instituto Superior Técnico Para a Investigação e Desenvolvimento, Av. António José de Almeida nº12, 1000-043 Lisboa, Portugal*

microorganisms on surfaces, but their technological development has not yet reached enough maturity.[5] The selection of an appropriate antifouling agent is crucial for the coating's performance, particularly in the early stages of biofouling development, such as microfouling and biofilm formation, where antimicrobial and anti-biofilm activities play a key role. This choice depends on the agent's chemical reactivity, antimicrobial efficacy, and ecotoxicity, as these properties influence both its immobilization on surfaces and overall effectiveness.[6] Azamacrocycle derivatives, in particular cyclam-based metal complexes, are of special interest within this context due to their antimicrobial properties.[7] Additionally, cyclam ligands provide a strong stabilizing effect, which enhances metal coordination and thus control over metal ion release.[7e] Immobilization within a polymeric coating matrix reinforces stabilization, potentially improving sustainability compared with conventional copper-based or biocide-releasing antifouling systems. Previous studies have shown that the presence of iron within polyurethane matrices can confer antimicrobial and anti-biofilm properties. In particular, polyurethane-coated surfaces incorporating cyclam-based Fe(III) complexes with the formula [{$R_2(^{4\text{-}CF3}PhCH_2)_2$Cyclam}$FeCl_2$]Cl (R = H, $HOCH_2CH_2CH_2$) significantly reduce both culturable and total *C. marina* biofilm cells compared to polyurethane-coated control surfaces.[8] This reduction was accompanied by decreases in biofilm surface coverage, thickness, and biovolume, indicating effective antifouling performance at multiple levels of biofilm development.

A recent study by Robinson *et al.*[9] demonstrated that cyclen-based Cu(II) complexes incorporated into silica and epoxy-based marine paint formulations showed limited bactericidal activity, likely due to insufficient surface copper concentration, and also highlighted that the ligands may themselves contribute to biofilm inhibition even in the absence of metal ions.

Altogether, these studies indicate that coatings incorporating cyclam-based metal complexes can provide effective antifouling activity through multiple mechanisms, including both metal-mediated antimicrobial effects and ligand-mediated inhibition of biofilm formation. When compared with existing antifouling strategies, such as copper-containing and hybrid metal-based coatings displaying antimicrobial performance under laboratory and field conditions, cyclam–metal systems offer a promising alternative. However, the limited bactericidal activity observed in some Cu(II)-based formulations and the potential to further optimize metal stabilization by refining ligand design, metal incorporation, and the compatibility of cyclam–metal systems with polymeric matrix interactions emphasize that significant improvements are still needed. The derived functional coatings could achieve enhanced, sustained antifouling efficacy while minimizing environmental impact, addressing the ongoing challenge of balancing effectiveness and sustainability in marine coatings.

Following previous studies on cyclam-based Fe(III) and Cu(II) complexes, in this work, we report the synthesis and characterization of polyurethane-coated surfaces incorporating Cu(II) and Fe (III) complexes stabilized within the $(HOCH_2CH_2)_2(^{4\text{-}CF3}PhCH_2)_2$Cyclam framework, and the assessment of their potential to further enhance antifouling activity against *C. marina* biofilm formation.

Results and discussion

Synthesis and characterization of cyclam-based complexes

The *trans*-disubstituted cyclam $H_2(^{4\text{-}CF3}PhCH_2)_2$Cyclam, **1**, reacts with ethyl bromoacetate to give the tetrasubstituted species $(EtOOCCH_2)_2(^{4\text{-}CF3}PhCH_2)_2$Cyclam, **2**. Upon reaction with $LiAlH_4$, compound **2** is converted into $(HOCH_2CH_2)_2(^{4\text{-}CF3}PhCH_2)_2$Cyclam, **3**, as shown in Scheme 1.

The ^{1}H NMR spectra of compounds **2** and **3** (Fig. S1A and S2A, respectively, SI) show five multiplets for the methylene protons of the cyclam ring, each integrating to four protons, along with a set of resonances corresponding to protons of the $^{4\text{-}CF3}PhCH_2$, $EtOOCCH_2$, and $HOCH_2CH_2$ pendant arms of the macrocycle. The benzylic protons of the $^{4\text{-}CF3}PhCH_2$ pendant arms are observed as singlets at 3.59 and 3.65 ppm in compounds **2** and **3**, respectively, in accordance with nitrogen inversion. The hydroxyl protons of the $HOCH_2CH_2$ pendant arms present in **3** appear at 4.73 ppm. The ^{19}F NMR spectra of compounds **2** and **3** show a single resonance for the CF_3 groups at −62.4 ppm. The $^{13}C\{^1H\}$ NMR spectra of compounds **2** and **3** (Fig. S1B and S2B, respectively, SI) are in accordance with the patterns observed in the ^{1}H spectra and, thus, in agreement with C_{2v} symmetry in solution.

Crystals of **2** and **3** suitable for single-crystal X-ray diffraction were obtained by slow evaporation of chloroform solutions. The ORTEP diagrams of the solid-state molecular structures of compounds **2** and **3** are shown in Fig. 1 and 2, respectively. The overall molecular shape of the macrocycles is remarkably flat and disk-like, with the four nitrogen atoms coplanar, as observed in other tetrasubstituted cyclams.[10] The N(1)···N(1#) and N(2)···N(2#) transannular distances are 5.391 and 5.133 Å for **2** and 5.557 and 4.891 Å for **3**. These values correspond to cavity sizes smaller than 2.133 and 1.891 Å for **2** and **3**, respectively, calculated from the sum [1.5 + 1.5] = 3.0 Å of the van der Waals radii of the two nitrogen atoms.[11] These values are in the same range as those observed in other tetrasubstituted cyclams.[10]

The structural arrangement of the macrocycle framework in **3** is determined by intramolecular hydrogen bonds between O(1)–H(1O) and N(1) with distances of 2.163 Å that form two 8-membered heterocycles. A similar arrangement is observed in [{$(HOCH_2CH_2CH_2)_2(R)_2$Cyclam}] (R = $PhCH_2$ and $^{4\text{-}CF3}PhCH_2$) where intramolecular hydrogen bonds between the hydroxyl groups and the nitrogen atoms form 9-membered heterocycles ($d_{OH\cdots N}$ = 1.97–2.20 Å).[10a]

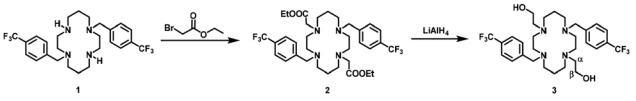

Scheme 1 Synthetic route for the preparation of $(HOCH_2CH_2)_2(^{4\text{-}CF3}PhCH_2)_2$Cyclam, **3**.

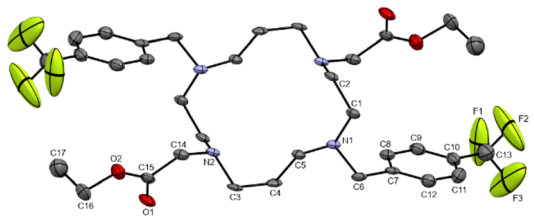

Fig. 1 ORTEP diagram of $(EtOCCH_2)_2(^{4\text{-}CF3}PhCH_2)_2Cyclam$, **2**, showing thermal ellipsoids at the 40% probability level. Hydrogen atoms are omitted for clarity.

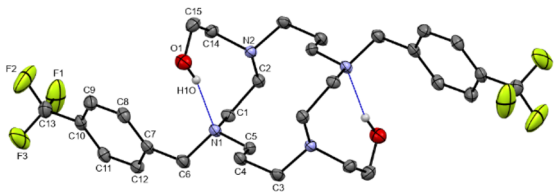

Fig. 2 ORTEP diagram of $(HOCH_2CH_2)_2(^{4\text{-}CF3}PhCH_2)_2Cyclam$, **3**, showing thermal ellipsoids at the 40% probability level. Selected hydrogen atoms are omitted for clarity. Dashed blue lines represent hydrogen bonds.

Compound **3** reacts with $Cu(CH_3COO)_2{\cdot}H_2O$ and $FeCl_3$ to yield complexes of formula $[\{(HOCH_2CH_2)_2(^{4\text{-}CF3}PhCH_2)_2Cyclam\}Cu](CH_3COO)_2$, **4**, and $[\{(HOCH_2CH_2)_2(^{4\text{-}CF3}PhCH_2)_2Cyclam\}FeCl_2]Cl$, **5**, as shown in Scheme 2.

The IR spectra of complexes **4** and **5** (Fig. S3 and S4, respectively, SI) show broad absorption bands due to the hydroxyl groups of the $HOCH_2CH_2$ pendant arms of the cyclam ring at 3362 and 3305 cm^{-1}, respectively. The vibrational bands assigned to the C–F bond stretching of $-CF_3$ groups appear at 1119 and 1066 cm^{-1} in **4** and at 1107 and 1066 cm^{-1} in **5**. The band at 1323 cm^{-1} present in both complexes is assigned to the combination of ν_{C-C} and ν_{C-N} modes characteristic of the stretching vibrational bands of C–C and C–N modes (1400–1000 cm^{-1}).[12] Strong absorption stretching vibration bands at 1568 and 1390 cm^{-1} are assigned to $\nu_{C=O}$ and ν_{C-O}, respectively, due to the acetate anions in **4**. The molar conductivity value obtained for complex **4** of 240 Ω^{-1} cm^2 mol^{-1} represents the behaviour of a 2 : 1 electrolyte,[13] consistent with the presence of the $[\{(HOCH_2CH_2)_2(^{4\text{-}CF3}PhCH_2)_2Cyclam\}Cu]^{2+}$ cation and two acetate counterions in solution.

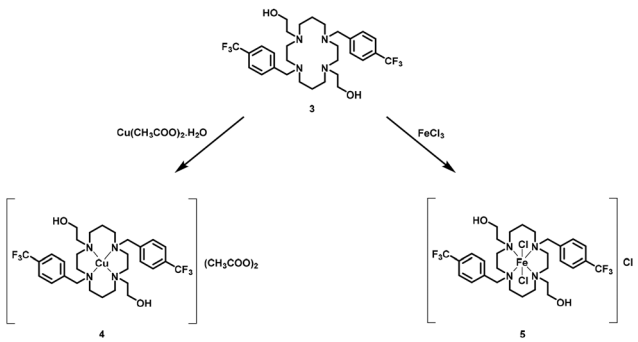

Scheme 2 Synthesis of $[\{(HOCH_2CH_2)_2(^{4\text{-}CF3}PhCH_2)_2Cyclam\}Cu](CH_3COO)_2$, **4** and $[\{(HOCH_2CH_2)_2(^{4\text{-}CF3}PhCH_2)_2Cyclam\}FeCl_2]Cl$, **5**.

The ^{57}Fe Mössbauer spectrum of complex **5** obtained at 80 K exhibits two quadrupole doublets with sharp peaks (Fig. S5, SI). The estimated isomer shifts, IS, relative to α-Fe at room temperature and quadrupole splitting, QS, (Table S1, SI) are consistent with two Fe^{III} species, one with high-spin, HS, (S = 5/2) and the other with low-spin, LS, (S = 1/2) configurations that correspond to *cis* and *trans* isomers, respectively, as explained in detail for the previously reported structural characterization of $[\{H_2(^{4\text{-}CF3}PhCH_2)_2Cyclam\}FeCl_2]Cl$.[7e] The differences in QS observed for the low-spin (LS) Fe^{III} species can be attributed to the higher sensitivity of their QS to environmental changes compared to high-spin (HS) Fe^{III}. The electric field gradient (efg) for HS Fe^{III} is only due to the electric charge distribution in the lattice since the d orbitals are evenly occupied. The QS of the LS Fe^{III} has a stronger contribution due to the uneven population of d orbitals. In a distorted octahedral coordination, the t_{2g} orbitals with higher energy have a lower electron population than the remaining t_{2g} orbitals. The variation of ligand composition and geometry promotes different distortions of the octahedral coordination, leading to differences in the efg created by the electronic distribution in LS Fe^{III} and consequently to larger variations of their quadrupole splittings when compared to HS Fe^{III}.[14]

Biofilm development on polyurethane-modified coating surfaces

The effect of polyurethane-modified surfaces containing compounds **3**, **4** and **5**, on 56-day-old *C. marina* biofilms, formed under defined hydrodynamic conditions that mimic natural marine environments, was first evaluated by Optical Coherence Tomography (OCT). Quantitative data obtained from OCT analysis for different biofilm parameters, including biofilm thickness, total biofilm volume, and biofilm porosity, are represented in Fig. 3. The average thickness of biofilms developed on the control surface (**PU**) was 244 ± 13 μm.

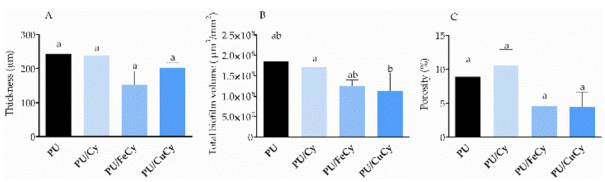

Fig. 3 Biofilm thickness (A), total biofilm volume (B), and biofilm porosity (C) of 56-day-old *C. marina* biofilms developed on different PU surfaces (**PU**, **PU/Cy**, **PU/CuCy**, and **PU/FeCy**). The mean and SD from two biological assays with two technical replicates each are represented. Significant differences between surfaces were considered for p values <0.05 and represented by different lowercase letters.

Biofilms formed on the polyurethane coating surface containing compound **3** (**PU/Cy**) exhibited a similar thickness to those formed on the control surface. On the other hand, the thickness of biofilms formed on the polyurethane coating surfaces containing compounds **4** (**PU/CuCy**) and **5** (**PU/FeCy**) decreased by 17% and 38%, respectively, with no statistically significant differences observed (Fig. 3A). Likewise, the total biofilm volume decreased by 39% and 33% for biofilms formed on the **PU/CuCy** and **PU/FeCy** surfaces, respectively, compared to the **PU** control (Fig. 3B; $p = 0.11$ and $p = 0.10$, respectively). Regarding biofilm porosity, biofilms formed on the **PU/Cy** surface exhibited a slight increase in porosity (approximately 11%), while biofilms formed on the **PU/CuCy** and **PU/FeCy** surfaces showed a decrease in porosity by 50% and 48%, respectively, compared to the **PU** control. However, these differences were not statistically significant.

Fig. 4 and 5 show representative 2D and 3D OCT images, respectively, of 56-day-old *C. marina* biofilms, supporting the quantitative data presented in Fig. 3.

In general, biofilms formed on the control and PU-modified surfaces displayed a heterogeneous architecture, with large biofilm streamers reaching up to 500 μm on the **PU**, **PU/Cy** and **PU/CuCy** surfaces (Fig. 5). These biofilm structures may affect local hydrodynamics and increase the surface area of the biofilm in contact with the surrounding environment, facilitating the access of nutrients and oxygen to the biofilm cells, thereby promoting its growth.[15]

On the other hand, a reduced thickness was observed in biofilms formed on the **PU/FeCy** surface, while a notable decrease in total biofilm volume was evident on both the **PU/CuCy** and **PU/FeCy** surfaces (Fig. 4 and 5).

Moreover, the qualitative 2D OCT images confirm a higher presence of empty spaces (pores) in biofilms formed on the **PU/Cy** surface compared to those on PU surfaces containing compounds **4** and **5** (**PU/CuCy** and **PU/FeCy**, respectively), as highlighted in blue in Fig. 4.

The potential of PU-modified surfaces to mitigate 56-day-old *C. marina* biofilm development was also evaluated by quantifying the number of total and culturable biofilm cells (Fig. 6). The number of total biofilm cells on **PU/Cy** and **PU/FeCy** surfaces was similar to those on the control **PU** surface (Fig. 6A). Interestingly, a significant decrease of 24% in biofilm cell count was observed on the **PU/CuCy** surface compared to **PU** ($p < 0.05$). Moreover, a reduction in culturable biofilm cells was observed on all PU-modified surfaces compared to the control surface, which showed $1.03 \times 10^9 \pm 2.18 \times 10^8$ CFUs per cm^2 (Fig. 6B). Biofilms formed on the **PU/Cy** surface showed a 41% reduction in culturable cells ($p < 0.05$), whereas biofilms on **PU/CuCy** and **PU/FeCy** surfaces exhibited average decreases of 36% and 39%, respectively ($p > 0.05$). However, no significant differences in the number of culturable biofilm cells were observed among the three PU-modified surfaces. These results demonstrate the antimicrobial potential of PU-modified surfaces against *C. marina* biofilms.

In general, all PU-modified surfaces tend to reduce the biofilm thickness, total biofilm volume, and the number of culturable *C. marina* biofilm cells (Fig. 3A and B and 6B). Although some of the differences between PU-modified surfaces and the control surface for certain biofilm parameters are not statistically significant, they indicate that the cyclam-based complexes have the potential to reduce biofilm formation under the tested conditions. This makes them promising compounds for marine applications, where even minor reductions in biofouling can yield substantial economic and environmental benefits, as a biofouling layer as thin as 0.5 mm can increase greenhouse gas emissions by up to 25%.[16]

The **PU/FeCy** surface showed the highest reduction in biofilm thickness (38%, Fig. 3A), and similar reductions in total biofilm volume and porosity to the **PU/CuCy** surface

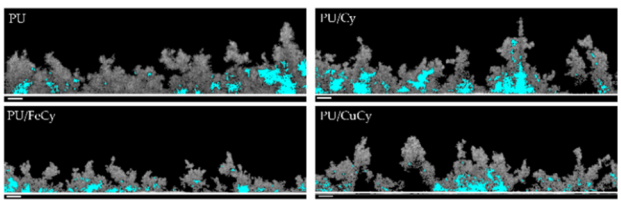

Fig. 4 Representative 2D cross-sectional OCT images of 56-day-old *C. marina* biofilms developed on **PU**, **PU/Cy**, **PU/CuCy**, and **PU/FeCy** surfaces. The biofilm is represented in grey, and the empty spaces in the biofilm structure are highlighted in blue (scale bar = 100 μm).

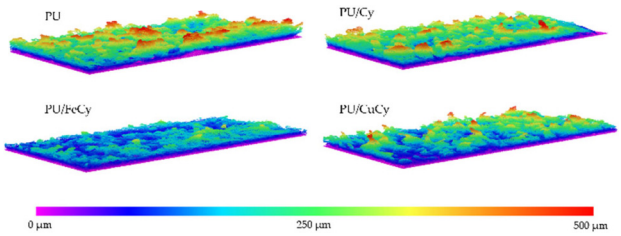

Fig. 5 Representative 3D cross-sectional OCT images of 56-day-old *C. marina* biofilms developed on **PU**, **PU/Cy**, **PU/CuCy**, and **PU/FeCy** surfaces. The colour scale represents biofilm thickness.

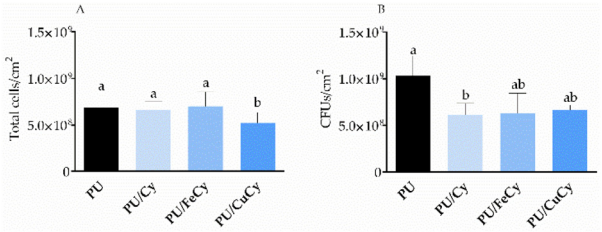

Fig. 6 Total (A) and culturable (B) biofilm cells of 56-day-old *C. marina* biofilms developed on different PU surfaces: **PU**, **PU/Cy**, **PU/CuCy**, and **PU/FeCy**. The mean and SD from two biological assays with two technical replicates each are represented. Significant differences between all surfaces were considered for p values <0.05 and represented by different lowercase letters.

(Fig. 3B and C). Additionally, the **PU/CuCy** surface exhibited the greatest reduction in the number of biofilm total cells (24%, Fig. 6B). On the other hand, the **PU/Cy** surface showed an increase in biofilm porosity compared to the control (Fig. 3C) and a significantly higher reduction in culturable biofilm cells ($p \leq 0.05$, 41%, Fig. 6A). Although biofilms formed on **PU/FeCy** and **PU/CuCy** surfaces showed a marked decrease in biofilm thickness (Fig. 3A) and total biofilm cells (Fig. 6A), respectively, indicating reduced biofilm growth on these surfaces, they presented lower porosity compared to the control (Fig. 3C). While the reduction in biofilm thickness and total biofilm cells is favourable for the performance of nautical equipment, the lower porosity may have a variable impact on biofilm development. In low-porosity biofilms, internal mass transfer may be hampered, impairing the metabolic activity of biofilm cells and limiting biofilm maturation. On the other hand, penetration into the inner layers of the biofilm of chemical compounds used for biofouling control may be hampered.[17] In contrast to what was observed in PU surfaces containing compounds **4** and **5**, the increased porosity of biofilms on the **PU/Cy** surface may facilitate these cleaning procedures.

The antimicrobial and antiadhesive effects of the **PU/CuCy** and **PU/FeCy** surfaces may be related to the incorporation of iron and copper into the PU coating formulation. A recent study performed by Carvalho *et al.*,[8] which investigated the potential of novel PU-based coatings containing cyclam-based Fe(III) complexes against 42-day-old *C. marin*a biofilms, showed that these surfaces reduced both total and culturable biofilm cells, as well as biofilm surface coverage, thickness, and biovolume. Similarly, a study performed by Kefallinou *et al.*[18] described "hybrid" silver and copper sputtered superhydrophobic surfaces that exhibited both bacterial repulsion and long-term bactericidal efficacy against the Gram-negative cyanobacterium *Synechococcus* sp. PCC7942. The antifouling potential of copper-based surfaces was also demonstrated in an *in situ* study conducted in Cartagena Bay, Chile (a fully exposed bay with incoming waves), in which two traditional copper-based antifouling coatings and a copper-based slow-release controlled-wear polymer antifouling paint showed low biomass and richness of micro- and macrofoulers after 12 months of exposure, highlighting the relevance of Cu-containing coatings in a real context.[19]

To assess the potential leaching of copper and iron from **PU/CuCy** and **PU/FeCy** surfaces, respectively, an Inductively Coupled Plasma Optical Emission Spectroscopy (ICP-OES) analysis was performed on water in contact with the coated surfaces exposed to water for 3, 7, 14, 21, 28, and 56 days. The results indicated that no metal leaching was detected in the analysed water samples, up to a limit of 5 ppb. These values indicate residual metal leaching from the PU-based marine coatings, suggesting potential long-term effectiveness and a low environmental impact, in accordance with the permissible limits for copper and iron in drinking water systems established by the World Health Organization (WHO).[20] On the other hand, the ecotoxicity of the cyclam-based Cu(II) and Fe(III) complexes, expressed as the 50% effective concentration (EC_{50}) against *Daphnia magna*, was determined to be 3.7 and 23.4 ppm, respectively. This supports the long-term effectiveness and low environmental impact of **PU/CuCy** and **PU/FeCy** surfaces, suggesting that PU-modified surfaces containing cyclam-based Cu(II) and Fe(III) complexes are suitable for marine applications.

Integrity of polyurethane-modified coating surfaces

To evaluate the integrity of PU-based coatings with time, **PU** control, **PU/Cy**, **PU/CuCy**, and **PU/FeCy** surfaces were analysed before and after 56 days of bacterial exposure by Fourier Transform Infrared Attenuated Total Reflectance (FTIR-ATR) spectroscopy and Atomic Force Microscopy (AFM). FTIR-ATR data reveal that the spectra of PU-based coatings containing compounds **4** and **5** (**PU/CuCy** and **PU/FeCy**, respectively) are similar to the spectrum of the polyurethane polymeric matrix (**PU** (control)), as shown in Fig. 7A. These IR spectra show characteristic bands assigned to the polyurethane material at 3344 cm^{-1} (the ν_{N-H} stretching vibration mode of the aliphatic amine groups of secondary urethanes), 3000–2800 cm^{-1} (ν_{C-H} asymmetric and symmetrical $-CH_2$ groups) and 1725 cm^{-1} ($\nu_{C=O}$ stretching of the ester carbonyl group of urethanes). Other characteristic bands could be assigned to polyurethanes, ranging from 1600 to 1500 cm^{-1} (ν_{N-H} out-of-plane bending and ν_{C-N} stretching modes) and from 1200 to 1100 cm^{-1} (ν_{C-O} stretching mode).[21]

Coating surfaces soaked for 56 days in water and bacterial media revealed no changes in the IR spectra (Fig. S6–S9), indicating that the main polymeric structure of coating surfaces is maintained during the tested period.

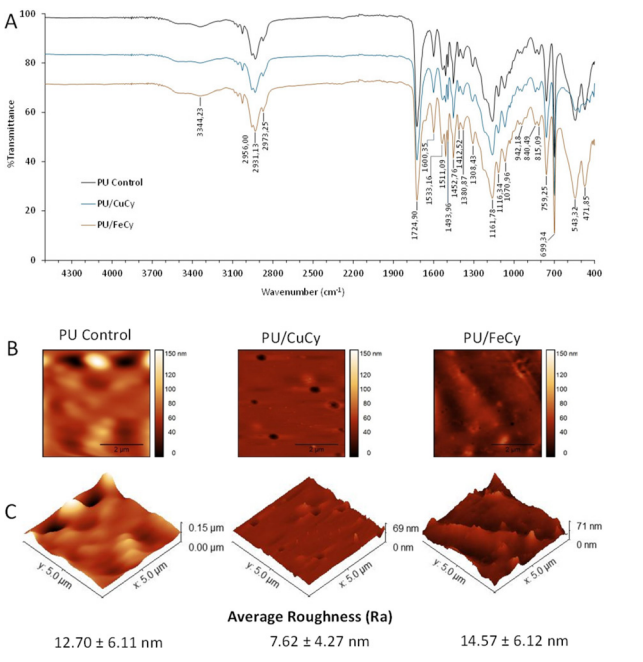

Fig. 7 FTIR-ATR spectra (A) and two-dimensional (B) and three-dimensional (C) AFM surface images of PU-based coatings, **PU** control, **PU/CuCy**, and **PU/FeCy** coating surfaces, including the arithmetic average roughness (R_a) values. All images correspond to a 5 × 5 μm^2 surface area.

The morphology of surfaces was also evaluated through optical images and two-dimensional and three-dimensional AFM images (Fig. 7B, C, and Tables S4, S5). The observations revealed different morphologies for the different formulations. The **PU/Cy** surface is the smoothest surface, followed by **PU/CuCy**, **PU**, and **PU/FeCy**, as supported by the average roughness (R_a) values, Fig. 7B and C, and Table S6. These differences are expected, as the different immobilized cyclam-based compounds introduce different physical–chemical interactions with the commercial formulations. Optical images (Table S4) also reveal features such as bumps, valleys, and pores generated during the paint application and solvent evaporation stages of the curing process. These features are the main contributors to the obtained R_q roughness parameter (Table S6).

After exposure to water and bacterial biofilms, changes occurred in the morphology of PU-based surfaces (Tables S4–S6), particularly expressed on the **PU** and **PU/CuCy**, and after exposure to the bacterial biofilm, associated with the release of paint components, typical of the early service life stage of solvent-based formulations,[22] leading to localised physical degradation and interactions with the biofilm. On the other hand, **PU/Cy** showed a more stable surface, probably due to its original smoother surface and fewer features detected.

Notably, these morphological changes did not affect the polymeric structure of the coatings at the chemical level, as confirmed by their FTIR-ATR spectra.

Materials and methods

General considerations

$H_2(^{4\text{-}CF3}PhCH_2)_2Cyclam$, **1**, was prepared according to an already described procedure.[23] Tetrahydrofuran was purchased from Fisher Scientific and refluxed over sodium-benzophenone and collected by distillation under an atmosphere of nitrogen. All other reagents were commercial grade and used without further purification. NMR spectra were recorded on a Bruker AVANCE II 300 or 400 MHz spectrometer at 296 K. ^1H and ^{13}C NMR spectra were referenced internally to residual solvent resonances and reported relative to tetramethylsilane (0 ppm). ^{19}F NMR was referenced to external CF_3COOH (−76.55 ppm). 2D NMR experiments such as ^1H–$^{13}C\{^1H\}$ HSQC and ^1H–^1H COSY were performed to make all the assignments.

Infrared spectra were acquired using an IRSpirit FTIR spectrometer (Shimadzu, Japan) equipped with a single-reflection diamond ATR crystal, operating in the 4000–400 cm^{-1} range at a resolution of 4 cm^{-1}. Elemental analyses (C, H, and N) were performed at the SSADS-CACTI UVIGO Laboratory, Spain, using a Thermo Finnigan EA1112 automatic analyser instrument. The molar conductance determination of **4** was performed on a 10^{-3} M methanolic solution using a Meter Lab Conductometer model CDM210 with a cell constant equal to 1 cm^{-1}.

Synthetic procedures

$(EtOOCCH_2)_2(^{4\text{-}CF3}PhCH_2)_2Cyclam$ (2). Compound **1** (1.20 g, 2.32 mmol) was dissolved in 160 mL of acetonitrile. Three equivalents of ethyl bromoacetate (0.80 mL) and potassium carbonate (0.99 g) were added, and the mixture was stirred for two days at room temperature. Water was added to promote phase separation, and the product was extracted with several portions of chloroform. The organic phases were combined, dried with anhydrous $MgSO_4$, and evaporated to dryness, affording the product in 81% yield (1.29 g, 1.87 mmol). ^1H NMR ($CDCl_3$, 400.1 MHz, 296 K): δ (ppm) 7.55 (d, $^3J_{H-H}$ = 8 Hz, 4H, *m*-Ph), 7.47 (d, $^3J_{H-H}$ = 8 Hz, 4H, *o*-Ph), 4.07 (m, $^3J_{H-H}$ = 7 Hz, 4H, OCH_2CH_3), 3.59 (s, 4H, $PhCH_2N$), 3.23 (s, 4H, OCH_2N), 2.76 (m, 4H, [C2]CH_2N), 2.66 (m, 4H, [C3]CH_2N), 2.56 (overlapping, 8H total, 4H, [C2]CH_2N and 4H, [C3]CH_2N), 1.67 (m, 4H, $CH_2CH_2CH_2$), 1.18 (t, $^3J_{H-H}$ = 7 Hz, 6H, OCH_2CH_3). $^{13}C\{^1H\}$ NMR ($CDCl_3$, 100.6 MHz, 296 K): δ (ppm) 171.6 (*C*=O), 129.3 (*o*-Ph), 125.2 (d, $^3J_{C-F}$ = 3 Hz, *m*-Ph), 60.3 (OCH_2CH_3), 59.0 ($PhCH_2N$) 55.5 (OCH_2N), 51.7 ([C3]CH_2N) 51.4 (overlapping, [C2]CH_2N and [C3]CH_2N), 51.0 ([C2]CH_2N), 24.8 ($CH_2CH_2CH_2$), 14.3 (OCH_2CH_3). ^{19}F NMR ($CDCl_3$, 376.5 MHz, 296 K): δ (ppm) −62.4 (s, CF_3). Anal. calcd for $C_{34}H_{46}F_6N_4O_4\cdot(H_2O)_2$: C, 56.34; H, 6.95; N, 7.73. Found: C, 56.99; H, 6.79; N, 7.80.

$(HOCH_2CH_2)_2(^{4\text{-}CF3}PhCH_2)_2Cyclam$ (3). Compound **2** (0.60 g, 0.87 mmol) was dissolved in dry THF and added dropwise to a THF suspension of $LiAlH_4$ (0.25 g). The mixture was refluxed overnight under an atmosphere of nitrogen. After cooling to room temperature, an aqueous solution of sodium tartrate (10%) and sodium hydroxide (5%) was added dropwise. The product was extracted with several portions of diethyl ether. The organic phases were combined and dried with anhydrous $MgSO_4$. The solution was filtered, and the solvent evaporated to dryness. The crude was washed with *n*-hexane and a few drops of diethyl ether were added to obtain the product as a white powder in 74% yield (0.39 g, 0.64 mmol). ^1H NMR ($CDCl_3$, 300.1 MHz, 296 K): δ (ppm) 7.58 (d, $^3J_{H-H}$ = 9 Hz, 4H, *m*-Ph), 7.51 (d, $^3J_{H-H}$ = 6 Hz, 4H, *o*-Ph), 4.73 (s, 2H, O*H*), 3.65 (s, 4H, $PhCH_2N$), 3.49 (t, $^3J_{H-H}$ = 2 Hz, 4H, β-CH_2), 2.62–2.45 (overlapping, 16H, [C3]CH_2N and [C2]CH_2N), 2.31 (t, $^3J_{H-H}$ = 2 Hz, 4H, α-CH_2), 1.76 (m, 4H, $CH_2CH_2CH_2$). $^{13}C\{^1H\}$ NMR ($CDCl_3$, 75.5 MHz, 296 K): δ (ppm) 142.1 (i-Ph), 130.1 (*o*-Ph), 129.6 ($^2J_{C-F}$ = 32 Hz, *p*-Ph), 125.2 ($^3J_{C-F}$ = 4 Hz, *m*-Ph), 124.0 ($^1J_{C-F}$ = 272 Hz, CF_3), 59.8 (β-CH_2), 59.3 ($PhCH_2N$), 54.2 (α-CH_2), 53.5 ([C3]CH_2N or [C2]CH_2N), 51.1 ([C3]CH_2N or [C2]CH_2N), 50.0 ([C3]CH_2N or [C2]CH_2N), 48.9 ([C3]CH_2N or [C2]CH_2N), 25.1 ($CH_2CH_2CH_2$). ^{19}F NMR ($CDCl_3$, 282.4 MHz, 296 K): δ (ppm) −62.4 (s, CF_3). Anal. calcd for $C_{30}H_{42}F_6N_4O_2$: C, 59.59; H, 7.00; N, 9.27. Found: C, 59.28; H, 7.55; N, 9.22.

$[\{(HOCH_2CH_2)_2(^{4\text{-}CF3}PhCH_2)_2Cyclam\}Cu](CH_3COO)_2$ (4). Compound **2** (280 mg, 0.46 mmol) was dissolved in methanol and one equiv. of $Cu(CH_3COO)_2\cdot H_2O$ (93 mg, 0.46 mmol) was added. The reaction mixture was refluxed overnight. The solvent was evaporated to dryness, and the obtained powder was washed with small portions of diethyl ether. The product was obtained as a blue powder in 80% yield (290 mg, 0.37 mmol). FT-IR (ATR, cm^{-1}): 3362 (ν_{O-H}), 1568 ($\nu_{C=O}$), 1390 (ν_{C-O}), 1119 and 1066 (ν_{C-F}). Anal. calcd for $C_{34}H_{48}CuF_6N_4O_6\cdot(H_2O)_5$: C, 46.60; H, 6.67; N, 6.39. Found: C, 46.34; H, 6.12; N, 6.53.

[{(HOCH$_2$CH$_2$)$_2$($^{4\text{-CF3}}$PhCH$_2$)$_2$Cyclam}FeCl$_2$]Cl (5). Compound **2** (250 mg, 0.41 mmol) was dissolved in a mixture of methanol/chloroform (5 : 1) and one equiv. of $FeCl_3$ (67 mg, 0.41 mmol) was added. The reaction mixture was left stirring overnight at room temperature. The solvent was evaporated to dryness and the obtained powder was washed with small portions of diethyl ether. The product was obtained as an orange powder in 83% yield (265 mg, 0.34 mmol). FT-IR (ATR, cm^{-1}): 3305 (ν_{O-H}), 1107 and 1066 (ν_{C-F}). Anal. calcd for $C_{30}H_{42}Cl_3F_6FeN_4O_2{\cdot}(H_2O)_3$: C, 43.89; H, 5.89; N, 6.83. Found: C, 43.45; H, 5.18; N, 6.70.

Mössbauer spectroscopy

The Mössbauer spectrum of **5** was recorded at 80 K in transmission mode using a conventional constant acceleration spectrometer and a 25 mCi ^{57}Co source in a Rh matrix. The velocity scale was calibrated using α-Fe foil. Isomer shifts, IS, are given relative to this standard at room temperature. The absorber was obtained by packing the powdered samples into a Perspex holder. The absorber thickness was calculated based on the corresponding electronic mass absorption coefficients for the 14.4 keV radiation.[24] Spectra were recorded using a bath cryostat with the sample immersed in He exchange gas. The spectra were fitted to Lorentzian lines using a non-linear least-squares method.

Single-crystal X-ray crystallography

Crystals of compounds **2** and **3** suitable for single-crystal X-ray diffraction were coated and mounted on a loop with Fomblin® oil. Data were collected using graphite-monochromated Mo-Kα radiation (λ = 0.71073 Å) on a Bruker AXS-KAPPA APEX II diffractometer (Bruker AXS Inc., Madison, WI, USA) equipped with an Oxford Cryosystem open-flow nitrogen cryostat at 150(2) K. Data were corrected for Lorentzian polarization and absorption effects using SAINT[25] and SADABS[26] programs. SIR2004[27] was used for structure solution and SHELXL-2014/7[28] was used for full-matrix least-squares refinement on F^2. These programs are included in the WINGX-Version 2023.1 program package.[29] The hydrogen atoms of the O*H* groups were located in the electron density map. The other hydrogen atoms were inserted in calculated positions and allowed to refine in the parent atom. Crystallographic and experimental details of data collection and crystal structure determination for compounds **2** and **3** are available in Table S2, SI. Illustrations of the molecular structures of **2** and **3** were made with MERCURY 2022.3.0.[30]

Formulation of PU-based coatings

Complexes **3**, **4**, and **5** were incorporated into a two-component commercial polyurethane (PU)-based marine paint (Table 1), following previously established methodologies.[31] The paint system comprises the base resin F0032 and the curing agent 95 580 (Hempel, A/S, Copenhagen, Denmark). For the preparation of PU-based formulations, compounds were dissolved in tetrahydrofuran (≥99.8%, Fisher Chemical) (**3**), dioxane (≥99.5%, Sigma-Aldrich) (**4**) or *N*-methyl pyrrolidone (99.5%, Acros Organics) (**5**) at a compound/solvent weight ratio ranging from 0.24 to 0.27. These solutions were further added and blended into the PU-based paint components in exact amounts to yield a compound content of approximately 2.0 wt% in the wet and uncured coating formulations (Table 1). The weight ratio of the base resin to the curing agent was optimized following the supplier's recommendations.

Table 1 Marine coating formulations containing cyclam-based compounds

Coating formulation	Base/curing agent ratio (v/v)	Compound content (wt%)	Compound/solvent ratio (m/m)
PU (control)	9.0 ± 0.1	—	—
PU/Cy	8.7 ± 0.1	1.86 ± 0.02	0.24 ± 0.01
PU/CuCy	9.0 ± 0.1	1.89 ± 0.02	0.27 ± 0.01
PU/FeCy	8.4 ± 0.1	2.04 ± 0.02	0.27 ± 0.01

PU = polyurethane-based marine paint.

Substrate coating (coated coupons)

The resulting PU/compound-based formulations were used to coat 1 cm^2 acrylic substrates (Probalplás, Portugal) using a 4-sided film applicator with a reservoir (TQC Sheen). The substrate was coated in a single step, achieving a 200 μm film thickness using the appropriate side of the applicator, and then cured at room temperature (23 ± 2 °C) for about one week to ensure complete curing of the polymeric coating matrix.

Bacterial strain and culture preparation

The Gram-negative bacterium *Cobetia marina* (DSMZ 4741), obtained from the Leibniz Institute DSMZ—German Collection of Microorganisms and Cell Cultures (Braunschweig, Germany), was used as a model organism for marine biofilm development.[32] *C. marina* colonies grown on the complex salt-rich Våatanen Nine Salt Solution (VNSS) marine medium supplemented with 15 g L^{-1} agar (VWR International, Leuven, Belgium) were inoculated into 100 mL of the VNSS medium. After overnight incubation at 25 °C and 120 rpm (Agitorb 200ICP, Norconcessus, Ermesinde, Portugal), the inoculum was centrifuged for 10 min at 3100*g* (Eppendorf Centrifuge 5810R, Eppendorf, Hamburg, Germany). The pellet was then resuspended in fresh VNSS medium, and the bacterial suspension was adjusted to a final concentration of 1 × 10^8 cells per mL (OD_{610nm} = 0.2) using a V-1200 spectrophotometer (VWR International China Co., Ltd, Shanghai, China) to perform the biofilm assays.

C. marina biofilm development

Biofilm development was conducted over 56 days under controlled hydrodynamic conditions that mimic marine environments using 12-well microtiter plates (VWR International, Carnaxide, Portugal).[15a] *C. marina* biofilms were formed on the control surface (**PU**) and the modified surfaces: **PU/Cy**, **PU/CuCy**, and **PU/FeCy**. Firstly, 12-well polystyrene plates with transparent double-sided tape glued on each well and down-

facing coupons (1 cm^2) were subjected to UV sterilization for 30 min. Following that, the surfaces were fixed to the wells facing upward and subjected to another UV sterilization cycle. The adjusted *C. marina* suspension was added to each well. Control wells containing fresh VNSS were used to visually confirm the sterility of the assays while handling the microplates in a sterile environment throughout the experiments. In addition, the biofilm species composition was confirmed by observing colony-forming units (CFU) and analysing cell population features using flow cytometry (side scatter *versus* forward scatter signals) at the start of the assays and at the endpoint. The microplates were incubated at 25 °C and 185 rpm in an orbital shaker with a 25 mm diameter (Agitorb 200ICP, Norconcessus, Ermesinde, Portugal), achieving an average shear rate of 40 s^{-1}. This value is equivalent to the shear rate value for a ship in a harbour, and this setup has been shown to predict the biofouling patterns observed during extended sea immersion of surfaces.[33] Over the 56 days of biofilm development (the accepted minimum maintenance interval for economically viable underwater monitoring systems), the culture medium was replaced twice a week.[15a,34] A total of four replicates (two biological assays with two technical replicates each) were analysed.

C. marina biofilm analysis

After 56 days, biofilms developed on the control (**PU**) and PU-modified surfaces (**PU/Cy**, **PU/CuCy**, and **PU/FeCy**) were characterized using optical coherence tomography to assess biofilm thickness, total biofilm volume, and biofilm porosity. Subsequently, the number of total and culturable biofilm cells was determined by flow cytometry (FC) and colony-forming unit (CFU) enumeration, respectively.

Ecotoxicity assays

The ecotoxicity of **CuCy** and **FeCy** complexes was evaluated using the *Daphnia magna* acute immobilization test, following the ISO 6341:2012 standard.[35] The tests were conducted in the accredited Laboratório de Análises do Instituto Superior Técnico in Lisbon, Portugal. Ecotoxicity was quantified as the effective concentration (EC_{50}), representing the concentration at which 50% of the test organisms exhibited a defined toxic effect.

Optical coherence tomography

Following incubation, the culture medium was removed, and the microplate wells were washed with sterile NaCl solution (8.5 g L^{-1}) to eliminate loosely attached bacteria. A fresh sterile NaCl solution was then added to each well before OCT analysis. 2D and 3D OCT acquisitions of 56-day-old *C. marina* biofilms developed on the different surfaces were performed using a Thorlabs Ganymede Spectral Domain OCT system with a central wavelength of 930 nm (Thorlabs GmbH, Dachau, Germany).[15a] Representative sections of the coupon surface were arbitrarily chosen, with a minimum of three images taken for each coupon to ensure the reliability and accuracy of the results. OCT images were analysed as previously described.[15b,36] Briefly, the base of the biofilm was determined by fitting a parabola and a hyperboloid to the 2D and 3D images, respectively, connecting the white pixels from light reflection on the substratum surface. A gray-value threshold was set to distinguish the biofilm from the background, based on the gray-value histogram of the selected region of interest.[37] The upper contour of the biofilm was defined as the pixel farthest from the bottom with gray values above the threshold and connected to the biofilm base. Objects not connected to the base were excluded from the biofilm structure analysis. The assessment of biofilm thickness, total biofilm volume, and biofilm porosity was performed as detailed in Romeu *et al.*[15b]

Quantification of total and culturable biofilm cells

Biofilms were detached from the surfaces by immersing the coupons in 2 mL of sterile NaCl solution and vortexing for 3 min. The number of total biofilm cells per cm^2 was determined through FC by acquiring 10 μL of the biofilm cell suspension at a flow rate of 10 μL min^{-1} (CytoFLEX V0-B3-R1, Beckman Coulter, Brea, CA, USA). The number of culturable biofilm cells per cm^2 was assessed by spreading the diluted bacterial suspensions on VNSS agar and incubating overnight at 25 °C for CFU counting.

Metal leaching assessment by inductively coupled plasma-optical emission spectroscopy (ICP-OES)

To evaluate potential metal leaching from PU-based coatings, the different surfaces were exposed to ultrapure water and incubated under biofilm formation conditions (25 °C, 185 rpm) for 3 (corresponding to the period after which the culture medium is replaced during biofilm formation assays), 7, 14, 21, 28, and 56 days (the total duration of biofilm assays).

Additionally, to account for potential microbial degradation contributing to metal release, surfaces were also exposed to ultrapure water in the presence of *C. marina* for 3 days. After incubation, the water in contact with surfaces was filtered using 0.22 μm filters (VWR International, Carnaxide, Portugal) and analysed using an ICP-OES equipped with a nebulizer system and optical emission spectroscopy for detection. The metal content in the water samples was quantified using calibration curves prepared for both copper and iron. All measurements were conducted in triplicate.

Statistical analysis

Data analysis was performed using GraphPad Prism® for Windows, version 6.01 (GraphPad Software, Inc., San Diego, California, USA). Data are presented as the mean and standard deviation. The D'Agostino-Pearson and Shapiro–Wilk normality tests were performed to evaluate data distribution. Differences in the number of total and culturable biofilm cells, biofilm thickness, total biofilm volume, and biofilm porosity between the different surfaces were evaluated using the unpaired, non-parametric Mann–Whitney test. Significant differences between the tested surfaces were considered for p values <0.05 and represented by different lowercase letters.

Surface characterization of coatings

The integrity and surface properties of PU-based coatings were evaluated before and after *C. marina* biofilm formation assays. **PU** control, **PU/Cy**, **PU/CuCy**, and **PU/FeCy** coatings were characterized using Fourier Transform Infrared Attenuated Total Reflectance (FTIR-ATR) spectroscopy, optical microscopy, and Atomic Force Microscopy (AFM). Following bacterial exposure, the same analyses were performed to assess possible physicochemical and morphological changes induced by prolonged biofilm development.

Biofilms were formed on the coated surfaces as previously described in detail in the section "*C. marina* biofilm development". After 56 days of incubation, the bacterial cells were removed before surface analysis by immersing the samples in 2 mL of sterile NaCl solution and vortexing for 3 minutes. Control samples exposed exclusively to ultrapure water under identical experimental conditions were processed and analysed in parallel.

Fourier transform infrared (FTIR) spectroscopy was used to confirm any chemical changes in the polymeric coatings. Spectra of the coated surfaces, after exposure to different conditions, were recorded.

The morphology of the surfaces was characterized using a Bruker Innova Atomic Force Microscope (AFM) in tapping mode under ambient conditions with HQ:NSC35/Hard/Al BS-C μmasch® tips. The surface roughness values were obtained using Gwyddion® software (version 2.67) and represent the average values calculated from measurements taken on three distinct areas of the sample.

Conclusions

The antifouling activity of polyurethane-coated surfaces incorporating new Cu(II) and Fe(III) complexes was evaluated to assess the influence of the metal centre on *C. marina* biofilm inhibition. This study demonstrated that polyurethane-based coatings containing cyclam-based Cu(II) and Fe(III) complexes effectively hamper *C. marina* biofilm development compared to unmodified polyurethane control surfaces. After 56 days under controlled hydrodynamic conditions that mimic marine environments, these modified surfaces showed a marked reduction in the *C. marina* biofilm growth, as evidenced by the analysis of biofilm thickness, total volume, and total and culturable biofilm cell counts. By effectively inhibiting biofilm development, polyurethane-modified surfaces containing cyclam-based Cu(II) and Fe(III) complexes offer a promising strategy for marine biofouling prevention. The performance of the new Cu(II) cyclam-based complex highlights the potential for new developments.

These studies also revealed negligible (<5 ppb) copper and iron leaching from coatings, suggesting a low ecotoxicity impact, which is a critical factor for enhancing their long-term protective effect and the environmental compatibility and therefore the sustainability of marine operations by reducing the frequency of maintenance, repairs, and material replacements. Nevertheless, further research is required to translate these findings into real-world field applications.

Author contributions

I. M. N. and L. G. A. performed the synthesis and characterization of the compounds. B. J. C. V. and J. C. W. analysed and interpreted the Mössbauer data. M. J. R. performed the biofilm assays and OCT data analysis and interpretation. A. P. C. performed AFM and optical analyses and interpretation. N. G. L. and E. R. S. developed the PU-based coating formulations and related characterization. M. J. R., R. T.-S., F. J. M., E. R. S. and L. G. A. wrote the original draft. F. J. M., E. R. S. and L. G. A. conceived the project and supervised and guided the design, analysis, and interpretation. All authors have read and agree to the published version of the manuscript.

Conflicts of interest

There are no conflicts to declare.

Data availability

The data supporting this article have been included as part of the supplementary information (SI). Supplementary information is available. See DOI: https://doi.org/10.1039/d5dt01700a.

CCDC 2431109 (**2**) and 2431110 (**3**) contain the supplementary crystallographic data for this paper.[38a,b]

Acknowledgements

This work was supported by national funds through FCT/MCTES (PIDDAC): NanoBioMitig project (https://doi.org/10.54499/2022.06149.PTDC), UIDB/00511/2020 (https://doi.org/10.54499/UIDB/00511/2020), UIDP/00511/2020 (https://doi.org/10.54499/UIDP/00511/2020), LA/P/0045/2020 (https://doi.org/10.54499/LA/P/0045/2020), UIDP/00100/2020 (https://doi.org/10.54499/UIDP/00100/2020), UIDB/00100/2020 (https://doi.org/10.54499/UIDB/00100/2020), LA/P/0056/2020 (https://doi.org/10.54499/LA/P/0056/2020), UID/04349/2020 (https://doi.org/10.54499/UIDB/04349/2020) and the National Infrastructure Roadmap, LTHMFL-NECL, LISBOA-01-0145-FEDER-022096. This work was also supported by UID/04046/2023 – Biosystems and Integrative Sciences Institute grant from FCT, Portugal. M. J. R. acknowledges the receipt of a junior researcher fellowship from the project 2022.05314.PTDC (BacAllFree). L.G.A. acknowledges the receipt of a researcher fellowship from the project 2022.06149.PTDC (NanoBioMitig). E. R. Silva acknowledges the Foundation for Science and Technology (FCT) through the Scientific Employment Stimulus CEECIND/03530/2018/CP1553/CT0011

(https://doi.org/10.54499/CEECIND/03530/2018/CP1553/CT0011). R.T.-S. thanks FCT for the financial support of her work contract through the Scientific Employment Stimulus—Individual Call—2023.07999.CEECIND/CP2834/CT0014 (https://doi.org/10.54499/2023.07999.CEECIND/CP2834/CT0014). The authors also acknowledge the networking support from the COST Action-European MIC Network—New Paths for Science, Sustainability, and Standards (Euro-MIC), CA20130, supported by COST (European Cooperation in Science and Technology).

References

1 P. Vuong, A. McKinley and P. Kaur, *Mater. Degrad.*, 2023, **7**, 50.
2 (*a*) N. Hadžić, I. Gatin, T. Uroić and V. Ložar, *Ocean Eng.*, 2022, **245**, 110522; (*b*) Y. Wu, J. Hua and D. L. Wu, *Ocean Eng.*, 2022, **266**, 113038.
3 F. T. Chan, D. Ogilvie, F. Sylvester and S. A. Bailey, *Front. Mar. Sci.*, 2022, **9**, 808055.
4 (*a*) D. Björn, H. Blanck and M. Nydén, *Coastal Mar. Sci.*, 2010, **34**, 212–215; (*b*) J. Callow and M. Callow, *Nat. Commun.*, 2011, **2**, 244; (*c*) A. G. Nurioglu, A. C. C. Esteves and G. de With, *J. Mater. Chem. B*, 2015, **3**, 6547–6570; (*d*) Y. Gu, L. Yu, J. Mou, D. Wu, M. Xu, P. Zhou and Y. Ren, *Mar. Drugs*, 2020, **18**, 371; (*e*) M. J. Romeu and F. Mergulhão, *Microorganisms*, 2020, **11**, 1568.
5 A. M. C. Maan, A. H. Hofman, W. M. de Vos and M. Kamperman, *Adv. Funct. Mater.*, 2020, **30**, 2000936.
6 O. Ferreira, P. Rijo, J. F. Gomes, R. Santos, S. Monteiro, C. Vilas-Boas, M. Correia-da-Silva, S. Almada, L. G. Alves, J. C. Bordado and E. R. Silva, *ACS Sustainable Chem. Eng.*, 2020, **8**, 12.
7 (*a*) T. J. Hubin, P. N.-A. Amoyaw, K. D. Roewe, N. C. Simpson, R. D. Maples, T. N. C. Freeman, A. N. Cain, J. G. Le, S. J. Archibald, S. I. Khan, B. L. Tekwani and M. O. F. Khan, *Bioorg. Med. Chem.*, 2014, **22**, 3239; (*b*) M. O. F. Khan, J. Keiser, P. N.-A. Amoyan, M. F. Hossain, M. Vargas, J. G. Le, N. C. Simpson, K. D. Roewe, T. N. C. Freeman, T. R. Hasley, R. D. Maples, S. J. Archibald and T. J. Hubin, *Antimicrob. Agents Chemother.*, 2016, **60**, 5331; (*c*) I. Grabchev, S. Yordanova, E. Vasileva-Tonkova, M. Cangiotti, A. Fattori, R. Alexandrova, S. Stoyanov and M. Francesca, *Dyes Pigm.*, 2016, **129**, 71; (*d*) M. Spain, J. K.-H. Wong, G. Nagalingam, J. M. Batten, E. Hortle, S. H. Oehlers, X. F. Jiang, H. E. Murage, J. T. Orford, P. Crisologo, J. A. Triccas, P. J. Rutledge and M. H. Todd, *J. Med. Chem.*, 2018, **61**, 3595; (*e*) S. Almada, L. B. Maia, J. C. Waerenborgh, B. J. C. Vieira, N. P. Mira, E. R. Silva, F. Cerqueira, E. Pinto and L. G. Alves, *New J. Chem.*, 2022, **46**, 16764; (*f*) M. T. Branca, T. P. Silva, A. S. O. Lemos, L. M. Campos, T. F. Souza, C. Palazzi, V. S. Oliveira, E. S. Coimbra, F. O. N. Silva, A. C. F. B. Pontes, A. C. M. Apolônio, R. C. N. Melo, D. L. Pontes and R. L. Fabri, *ACS Omega*, 2025, **10**, 11386.
8 F. M. Carvalho, L. C. Gomes, R. Teixeira-Santos, A. P. Carapeto, F. J. Mergulhão, S. Almada, E. R. Silva and L. G. Alves, *Molecules*, 2025, **30**, 917.
9 H. Robinson, A. M. Daines, A. Brackovic, D. B. G. Williams, I. M. Sims and S. F. R. Hinkley, *Pure Appl. Chem.*, 2024, **96**, 549.
10 (*a*) A. Pilon, J. Lorenzo, S. Rodiguez-Calado, P. Adão, A. M. Martins, A. Valente and L. G. Alves, *ChemMedChem*, 2019, **14**, 770; (*b*) L. G. Alves, R. F. Munhá and A. M. Martins, *Chem. Heterocycl. Compd.*, 2021, **7**, 871; (*c*) I. M. Nunes, E. R. Silva and L. G. Alves, *Molbank*, 2024, **2024**, M1807.
11 L. Pauling, *The Nature of the Chemical Bond*, Cornell University Press, Ithaca, NY, USA, 2nd edn, 1948, pp. 187.
12 (*a*) G. D. Fleming, R. E. C. Clavijo, M. M. Campos-Vallete, M. S. Saavedra, S. Diez and R. Muñoz, *Vib. Spectrosc.*, 1997, **15**, 201; (*b*) D. Lin-Vien, N. B. Colthup, W. G. Fateley and J. G. Grasselli, *The handbook of infrared and Raman characteristic frequencies of organic molecules*, Academic Press, San Diego, USA, 1991; (*c*) K. Nakamoto, *Infrared and Raman Spectra of Inorganic and Coordination Compounds: Part B: Applications in Coordination, Organometallic, and Bioinoganic Chemistry*, John Wiley & Sons Inc., New Jersey, USA, 2008.
13 W. J. Geary, *Coord. Chem. Rev.*, 1971, **7**, 81.
14 G. M. Bancroft, *Mössbauer Spectroscopy: An Introduction for Inorganic Chemists and Geochemists*, McGraw Hill, London, 1973.
15 (*a*) M. J. Romeu, P. Alves, J. Morais, J. M. Miranda, E. D. de Jong, J. Sjollema, V. Ramos, V. Vasconcelos and F. J. M. Mergulhão, *Environ. Microbiol.*, 2019, **21**, 4411; (*b*) M. J. Romeu, M. Lima, L. C. Gomes, E. D. de Jong, J. Morais, V. Vasconcelos, M. F. R. Pereira, O. S. G. P. Soares, J. Sjollema and F. J. Mergulhão, *Polymers*, 2022, **14**, 4410; (*c*) M. J. Romeu, J. M. Miranda, E. D. de Jong, J. Morais, V. Vasconcelos, J. Sjollema and Filipe J. Mergulhão, *Biofilm*, 2024, **7**, 100204.
16 International Maritime Organization, *Preliminary results Impact of Ships' Biofouling on Greenhouse Gas Emissions*, 2021.
17 J. Sjollema, M. Rustema-Abbing, H. C. van der Mei and H. J. Busscher, *Appl. Environ. Microbiol.*, 2011, **77**, 5027.
18 D. Kefallinou, K. Ellinas, T. Speliotis, K. Stamatakis, E. Gogolides and A. Tserepi, *Coatings*, 2020, **10**, 25.
19 C. Arboleda-Baena, N. Osiadacz, M. Parragué, A. E. Gonzaléz, M. Fernández, G. R. Finke and S. A. Navarrete, *J. Mar. Sci. Eng.*, 2023, **11**, 217.
20 M. S. Braga, R. F. V. V. Jaimes, W. Borysow, O. F. Gomes and W. J. Salcedo, *Sensors*, 2017, **17**, 1730.
21 (*a*) B. C. Smith, *Spectroscopy*, 2023, **38**, 14; (*b*) S. Vlad, I. Spiridon, C. V. Grigoras, M. Drobota and A. Nistor, *e-Polymers*, 2009, **9**, 004.
22 C. Liang, B. Feng, S. Wang, B. Zhao, J. Xie, G. Huang, L. Zhu and J. Hao, *J. Hazard. Mater.*, 2024, **466**, 133668.
23 L. G. Alves, M. A. Antunes, I. Matos, R. F. Munhá, M. T. Duarte, A. C. Fernandes, M. M. Marques and A. M. Martins, *Inorg. Chim. Acta*, 2010, **363**, 1823.

24 G. J. Long, T. E. Cranshaw and G. Longworth, *Mössbauer Eff. Ref. Data J.*, 1983, **6**, 42.
25 *SAINT. Version 7.03A*, Bruker AXS Inc., Madison, WI, USA, 2003.
26 G. M. Sheldrick, *SADABS, Software for Empirical Absorption Corrections*, University of Göttingen, Göttingen, Germany, 1996.
27 M. C. Burla, R. Caliandro, M. Camalli, B. Carrozzini, G. L. Cascarano, L. D. Caro, C. Giacovazzo, G. Polidori and R. Spagna, *J. Appl. Crystallogr.*, 2005, **38**, 381.
28 G. M. Sheldrick, *Acta Crystallogr., Sect. C:Struct. Chem.*, 2015, **71**, 3.
29 L. J. Farrugia, *J. Appl. Crystallogr.*, 2012, **45**, 849.
30 C. F. Macrae, I. Sovago, S. J. Cottrell, P. T. A. Galek, P. McCabe, E. Pidcock, M. Platings, G. P. Shields, J. S. Stevens, M. Towler and P. A. Wood, *J. Appl. Crystallogr.*, 2020, **53**, 226.
31 O. Ferreira, P. Rijo, J. Gomes, R. Santos, S. Monteiro, R. Guedes, M. L. Serralheiro, M. Gomes, L. C. Gomes, F. J. Mergulhão and E. R. Silva, *Coatings*, 2021, **11**, 323.
32 (*a*) M. Lima, L. C. Gomes, R. Teixeira-Santos, M. J. Romeu, J. Valcarcel, J. A. Vázquez, M. A. Cerqueira, L. Pastrana, A. I. Bourbon, E. D. de Jong, J. Sjollema and F. J. Mergulhão, *Int. J. Mol. Sci.*, 2022, **23**, 14647; (*b*) F. Sousa-Cardoso, R. Teixeira-Santos, A. F. Campos, M. Lima, L. C. Gomes, O. S. G. P. Soares and F. J. Mergulhão, *Nanomaterials*, 2023, **13**, 381.
33 E. R. Silva, A. V. Tulcidas, O. Ferreira, R. Bayón, A. Igartua, G. Mendoza, F. J. M. Mergulhão, S. I. Faria, L. C. Gomes, S. Carvalho and J. C. M. Bordado, *Environ. Res.*, 2021, **198**, 111219.
34 S. Blain, J. Guillou, P. Tréguer, P. Woerther, L. Delauney, E. Follenfant, O. Gontier, M. Hamon, B. Leilde, A. Masson, C. Tartu and R. Vuillemin, *J. Environ. Monit.*, 2004, **6**, 569.
35 ISO 6341: 2012; *Water Quality-Determination of the Inhibition of the Mobility of Daphnia Magna Straus (Cladocera, Crustacea)*, International Organization for Standardization, Geneva, Switzerland, 2012.
36 S. I. Faria, R. Teixeira-Santos, M. J. Romeu, J. Morais, E. de Jong, J. Sjollema, V. Vasconcelos and F. J. Mergulhão, *Microorganisms*, 2021, **9**, 1102.
37 N. Otsu, *IEEE Trans. Syst. Man Cybern.*, 1979, **9**, 62.
38 (*a*) CCDC 2431109: Experimental Crystal Structure Determination, 2026, DOI: 10.5517/ccdc.csd.cc2mlrww; (*b*) CCDC 2431110: Experimental Crystal Structure Determination, 2026, DOI: 10.5517/ccdc.csd.cc2mlrxx.